LAWRENCE
LIVERMORE
NATIONAL
LABORATORY

UCRL-PROC-209551

Stifling of Crevice Corrosion in Alloy 22 During Constant Potential Tests

Kevin G. Mon, Pasu Pasupathi, Ahmet Yilmaz, Raúl B. Rebak

February 10, 2005

ASME Pressure Vessels & Piping Division Conference
Denver, CO, United States
July 17, 2005 through July 21, 2005

STIFLING OF CREVICE CORROSION IN ALLOY 22 DURING CONSTANT POTENTIAL TESTS

Kevin G. Mon

Pasu Pasupathi

Framatome/BSC
1211 Town Center Dr
Las Vegas, NV 89144

Ahmet Yilmaz

Raúl B. Rebak

Lawrence Livermore National Laboratory
7000 East Ave, L-631
Livermore, California, 94550 USA

ABSTRACT

Artificially creviced Alloy 22 (N06022) is susceptible to crevice corrosion in presence of high chloride aqueous solution when high temperatures and high anodic potentials are applied. The presence of oxyanions in the electrolyte, especially nitrate, inhibits the nucleation and growth of crevice corrosion. Crevice corrosion may initiate when a constant potential above the crevice repassivation potential is applied. The occurrence of crevice corrosion can be divided into three characteristic domains: (1) nucleation, (2) growth and (3) stifling and arrest. That is, crevice corrosion reaches a critical stage after which growth stops and the specimens start to regain the passive behavior displayed prior to localized attack.

Keywords: N06022, Crevice Corrosion, Stifling, Constant Potential

INTRODUCTION

Austenitic alloys such as Alloy 22 (N06022) that rely on the stability of a thin chromium oxide (Cr_2O_3) film for protection against corrosion are prone to crevice corrosion, a form of localized corrosion. Localized corrosion is an insidious type of attack, which forms at discrete sites on the surface and has a higher propagation rate than passive corrosion.

The susceptibility of an alloy to localized corrosion depends strongly on the composition of the electrolyte solution, temperature, and applied potential. In general, the environment becomes more aggressive with increases in chloride concentration, temperature, and applied potential. [1] Alloy 22 or N06022 is nickel-based (Ni) and contains by weight 22% chromium (Cr), 13% molybdenum (Mo), 3% tungsten (W) and approximately 3% iron (Fe). [2] Alloy 22 was commercially designed to resist the most aggressive industrial applications, offering a low general corrosion rate under both oxidizing and reducing conditions. [3] Under oxidizing and acidic conditions Cr exerts its beneficial effect in the alloy. Under reducing

conditions the most beneficial alloying elements are Mo and W, which offer a low exchange current for hydrogen discharge. [4,5]

Alloy 22 was selected as the outer shell material of the high level nuclear waste containers for the Yucca Mountain repository. [6,7] Several papers have been recently published describing the general and localized corrosion resistance of the Alloy 22 nuclear waste containers. [1,8-20] Cyclic Potentiodynamic Polarization (CPP) (ASTM G 61) [21] is a fast electrochemical test that can yield the crevice repassivation potential (e.g., ER1) for Alloy 22. Other electrochemical tests used included the Tsujikawa-Hisamatsu Electrochemical (THE) method and constant potential or potentiostatic (POT) tests. [20-21] A fourth type of electrochemical test, which also yields crevice repassivation potentials (e.g., ER2) is a combination of CPP and THE. [22] Below the repassivation potential determined using CPP or THE, crevice corrosion will not initiate. If a potential above the repassivation potential is applied, crevice corrosion may initiate.

Crevice Repassivation Potential of Alloy 22 in Chloride plus Nitrate Brines

The presence of nitrate (and other oxyanions) inhibits the nucleation and propagation of crevice corrosion in Alloy 22. [8-15,17-20, 22-23] It is necessary to have a minimum ratio of $[NO_3^-]/[Cl^-]$ in the order of 0.2 to 0.5 for the inhibition to be complete. [13,17,22] Table 1 shows the repassivation potentials for Alloy 22 in sodium chloride (NaCl) plus potassium nitrate (KNO_3) brines at 100°C. [23] Table 1 shows that for each base concentration of NaCl (1 m, 3.5 m and 6 m), as the amount of nitrate in the solution is increased, the repassivation potential (ER1) is increased. For example, for the 3.5 m NaCl solution, when the potassium nitrate concentration is raised from 0.175 m to 0.525 m, the repassivation potential increased from –110 mV SSC to –65 mV SSC (Table 1). Figure 1 shows CPP curves for two specimens in 6 m NaCl + 0.3 m KNO_3 solution at 100°C. Figure 1 shows the breakdown potential (E20) and the repassivation potentials (ER1 and ERCO). E20 is the potential at which the current density in the forward scan reaches 20 µA/cm². ER1 is the potential for which the current density in the reverse scan reaches 1 µA/cm². ERCO is the potential at which the forward and reverse scans in the CPP intersect (CO = cross over).

The objective of this research work was to determine if crevice corrosion will be initiated when a constant potential above the crevice repassivation potential is applied to an artificially creviced Alloy 22 specimen immersed in NaCl + KNO_3 brines at 100°C. Most of the tests were carried out at a constant potential of +100 mV SSC (Figure 1). The selected potential was between the breakdown potential (E20) and the repassivation potential (ER1) (Figure 1). Figure 1 was re-plotted using data originally reported in Reference 23.

EXPERIMENTAL

Alloy 22 specimens were prepared from 1-inch thick plate. There were several heats of material used in this research. The chemical composition of the most used specimens of Alloy 22 are given in Table 2. The specimens were prism crevice assemblies (PCA), which were fabricated based on the washer for crevice forming described in ASTM G 48 and G 78 [21] (Figure 2). The exposed surface area of the PCA specimen was 14.06 cm². The total area covered by the crevice formers was approximately 1.5 cm². All tested specimens were given a 600 grit surface finish and were degreased in acetone and treated ultrasonically for 5 minutes in de-ionized (DI) water 1 hour prior to testing. Specimens were used in the as-welded (ASW) condition. The weld was produced with matching filler metal using Gas Tungsten Arc Welding (GTAW). The welded specimens were not all weld metal but contained a weld seam, which varied in width from approximately 8 to 15 mm. The weld seam extended across the two surfaces of the specimen that were purposely creviced with the multiple tooth washer (Figure 2).

Electrochemical tests were carried out in deaerated solutions of NaCl + KNO_3 at 100°C. The pH of the solutions was approximately 6. Nitrogen (N_2) was purged through the solution at a flow rate of 100cc/min for 24 hours while the corrosion potential (E_{corr}) was monitored. Nitrogen bubbling was continued throughout all the electrochemical tests. The electrochemical tests were conducted in a one-liter, three-electrode, borosilicate glass flask (ASTM G 5). [21] A water-cooled condenser combined with a water trap was used to avoid evaporation of the solution and to prevent the ingress of air (oxygen). The temperature of the solution was controlled by immersing the cell in a thermostatisized silicone oil bath. All the tests were carried out at ambient pressure. The reference electrode was saturated silver chloride (SSC) electrode, which at ambient temperature has a potential of 199 mV more positive than the standard hydrogen electrode (SHE). The reference electrode was connected to the solution through a water-jacketed Luggin probe so that the electrode was maintained at near ambient temperature. The counter electrode was a flag (36 cm2) of platinum foil spot-welded to a platinum wire. All the potentials in this paper are reported in the SSC scale.

Basically the test sequence for each specimen consisted of three parts: (1) Ecorr evolution as a function of time for 24 h, (2) Polarization Resistance (ASTM G 59) three subsequent times and (3) A constant potential of +100 mV was applied for 168 h (1 week) while the current was monitored. After the tests, the specimens were examined in using both optical and scanning electron microscopy.

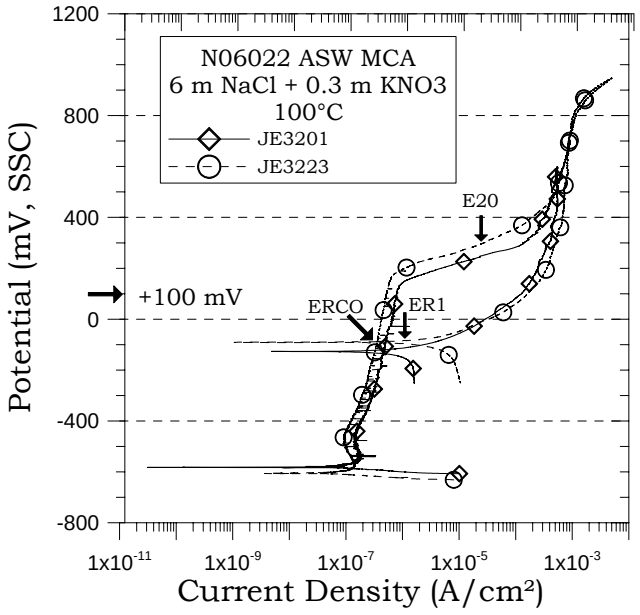

Figure 1. CPP for Alloy 22 at 100°C [23]

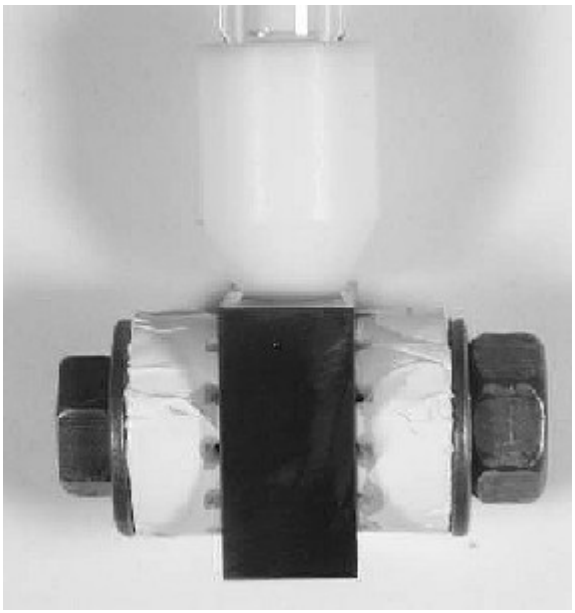

Figure 2. Creviced Specimen (PCA)

RESULTS AND DISCUSSION

Corrosion Potential and Corrosion Rate

Table 3 shows the list of tested specimens, the test electrolyte solutions and the results from the tests. The 24-h E_{corr} of the tested PCA specimens in the deaerated brines was in general low (below –400 mV SSC), except for specimen KE0110, which was –59 mV SSC. For specimen KE0110, crevice corrosion might have started at the free corroding potential since the repassivation potential for the tested conditions was in the same range as the measured E_{corr} (Table 1). Table 3 also shows that the corrosion rate for specimen KE0110 was also high, suggesting the onset of crevice corrosion before the constant potential was applied. The corrosion rate reported in Table 3 was calculated using the total specimen area of 14.06 cm², when the attack must have been occurred in the creviced regions (i.e., in a maximum area of 1.5 cm²). That is, the actual crevice corrosion rates might have been approximately ten times higher than the values reported in Table 3. The corrosion rate of specimen KE0166 was also higher than the expected. Both KE0110 and KE0166 did not show the initial passivity of the other tested specimens when the constant potential was later applied.

Potentiostatic (POT) or Constant Potential Tests

After an initial monitoring of the free corrosion potential in the deaerated brines for 24 hours and the polarization resistance tests, a constant potential was applied to the specimens listed in Table 3 for 1 week (168 h). The potential of choice was +100 mV since this potential was between the breakdown potential (E20) and the repassivation potential (ER1) in the cyclic potentiodynamic polarization curves (Figure 1). For specimen KE0164 the applied potential was 0 mV. Table 3 shows that for the eight tested specimens crevice corrosion was observed in the specimens after the completion of the tests. The base metal and in the weld seam were equally attacked during the tests (Figure 3). In most tests, the attack occurred under the 24 teeth of the crevice formers. In many cases, remnants of a black oxide were observed in and around the areas of the attack (Figure 3). These oxides are mostly molybdenum and tungsten oxide but may also contain chromium oxide. The attack of the metal was crystallographic in nature, revealing grain boundaries and crystal planes in the base metal and dendrite branches in the weld seam. Intergranular attack (IGA) occurred in the base metal (Figure 4) and interdendritic attack (IDA) in the weld seam (Figure 5). These types of attack are consistent with the exposure of Alloy 22 to a hot hydrochloric acid solution. There was no attack or corrosion outside the 24 crevice formers (CF).

Current Transients during POT Tests

During the potentiostatic tests, the output current was recorded as a function of time. In most of the tested specimens in Table 3, the current transients consisted of three domains (Figure 6). In Domain 1, the current decreased as a function of time suggesting that the specimen was developing a protective oxide film on the surface and therefore becoming passive.

Domain 1 is the crevice corrosion induction time. The average length of Domain 1 for all the tested specimens was 0.5 h (30 min.), which represents 0.3% of the total testing time (Table 4). In Domain 2, the current increased as a function of time until a maximum value was attained (Figure 6). The current then remained approximately constant or decreased. In Domain 2, crevice corrosion nucleated and developed. The average length of Domain 2 was 32 h, which represents 19% of the total testing time (Table 4). In Domain 3, the current decreased as a function of time showing repassivation of the crevice corrosion developed in Domain 2. In Domain 3, crevice corrosion stifled and died. The average time for Domain 3 was 135 h, which represents 81% of the total testing time (Table 4). That is, during most of the 168-h test the crevice was repassivating and was growing only 19% of the time. For all the other tests in Table 3 there were also three domains similar to Figure 6. In some cases Domain 1 was undistinguishable from Domain 2 (e.g., Specimen KE0110 in Figure 7). In many tests, at the end of Domain 3 the net current was cathodic suggesting that the reduction of protons and/or nitrate inside the crevice corroded area was more important than the dissolution of the metal.

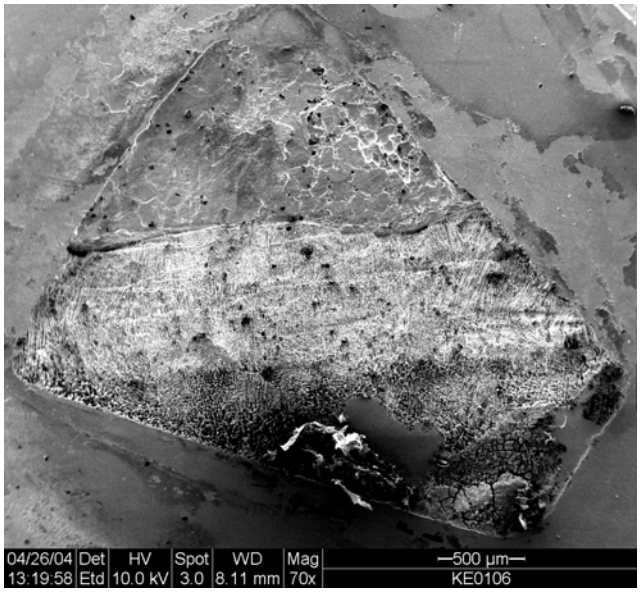

Figure 3. Corrosion Under one Crevice Former in Specimen KE0106. The top triangle is base metal, lower part of the attack is the weld seam

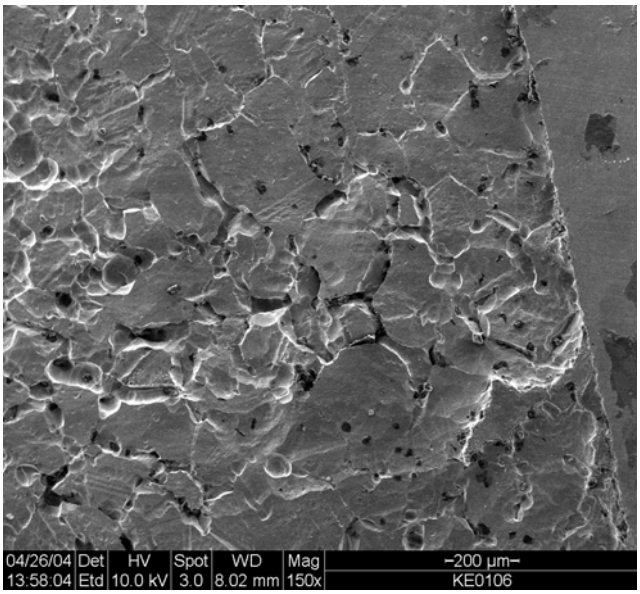

Figure 4. Detail of the IGA attack in the base metal

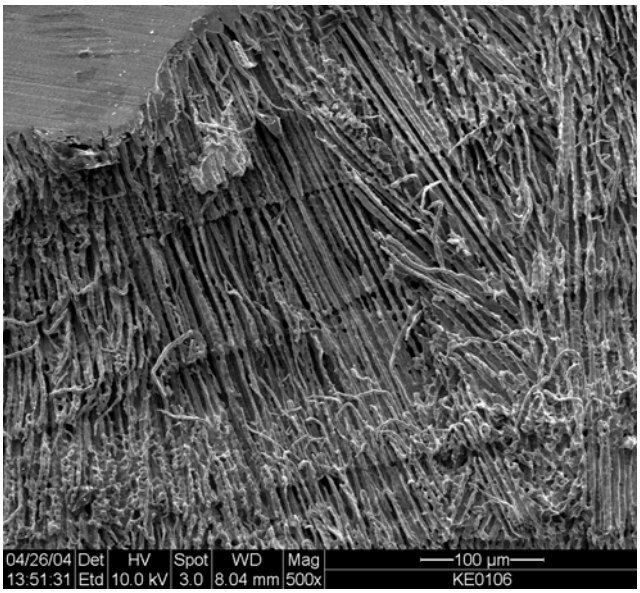

Figure 5. Detail of the IDA attack in the base metal

Extent of Crevice Corrosion in POT tests

During the constant potential tests, the amount of current that passed through the specimen represents the charge. That is, by integrating the curves (e.g., Figures 6 and 7) that represent the eight constant potential tests, the amount of dissolved material can be calculated. The total charge (in Coulombs) for all the tests is given in Table 5 along with the total dissolved

mass (in mg using and equivalent weight for Alloy 22 of 23.28 g). If it is assumed that crevice attack occurred uniformly under all 24 teeth (or spots) of the crevice former, the calculated depth of attack is between 14 µm and 59 µm (Table 5). That is, crevice corrosion stopped growing after just penetrating a few tens of microns into the metal. In all of the tested specimens, at least some attack was observed under all 24 crevicing-teeth. If it is conservatively assumed that crevice attack occurred under only one of the 24 teeth of the crevice former, the calculated depth of attack is between about 400 µm and 1,400 µm (Table 5). Thus, even using a very conservative treatment, the calculated depth of attack is less than 2 mm before stifling occurs.

Table 5 shows that, for the same applied potential and temperature, in the 3.5 m NaCl solution, the amount of dissolved metal was approximately twice as much for the lower nitrate containing solution (KE0108 and KE0106) than for the higher nitrate containing solution (KE0104 and KE0166). A similar trend is also found for the 6 m NaCl based solution (KE0105 and KE0164 vs. KE0103 and KE0110). Comparing the specimens with the same nitrate to chloride ratio at different base concentration of chloride (e.g., 3.5 m vs. 6 m) it appears that the more concentrated solution (6 m) dissolved less material than the less concentrated solution (3.5 m). It is possible that the higher ionic concentration of salt decreases the activity of water and therefore decreases the aggressiveness of the solution.

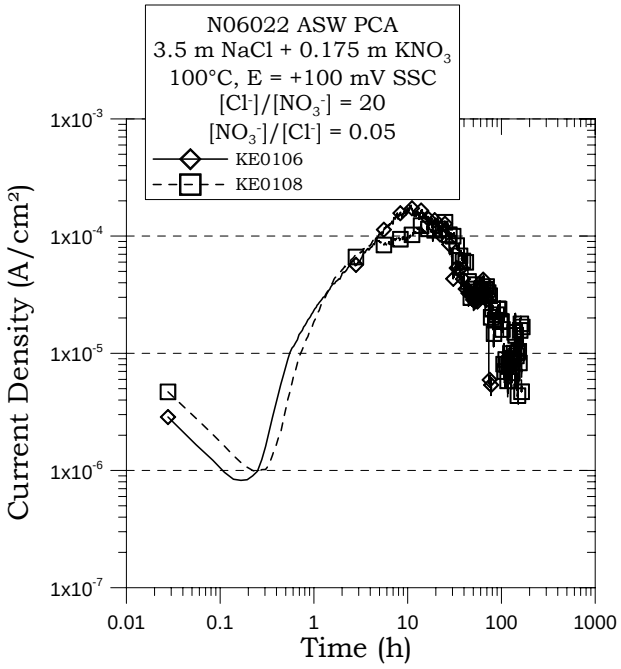

Figure 6. Current Transients during POT Tests

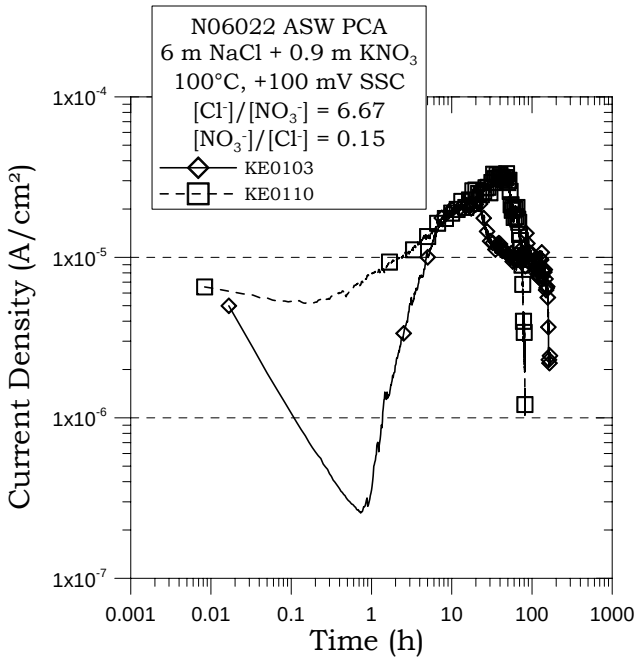

Figure 7. Current Transients during POT Tests

Power Laws for Crevice Corrosion

The three domains of current density vs. potential plots from the constant potential tests can be interpreted using a power law equation. For each test, the three domains were separately fit with power law equations. In Domain 1, the current density decreases as the time increases due to passivation (Figures 6-7). In a plot of logarithm of the current vs. logarithm of the time, the slope in Domain 1 should be a negative straight line.

$$i = A \cdot t^{n} \qquad \text{or}$$
$$\ln(i) = \ln A + n \cdot \ln(t) \qquad (1)$$

Where n is the slope in a plot such as Figure 8. The values of slopes in Domain 1 are listed in Table 4. In general, the slopes in Domain 1 varied between –0.6 and –1.0 (Table 4). The average slope for Domain 1 was –0.69, which is typical for passivation by the formation of a protective oxide film.

Figure 9 shows the plot of the current vs. time for a Domain 2. The current density increases following a power law similar to Equation 1. For Domain 2, the exponent n is positive and varied between 0.38 and 1.04 (Table 4). The average slope for Domain 2 was 0.72, which is typical for the growth and stifling of localized corrosion.

Figure 10 shows the plot of current vs. time for a Domain 3. Similar to Domain 1, the current density decreases as the time increases, showing progressive passivation of the crevice region. For Domain 3, the exponent n is negative and varied between –0.49 and –3.5 (Table 4). The average slope for Domain 3 was -1.89, which is more than twice as large as the slope for Domain 1.

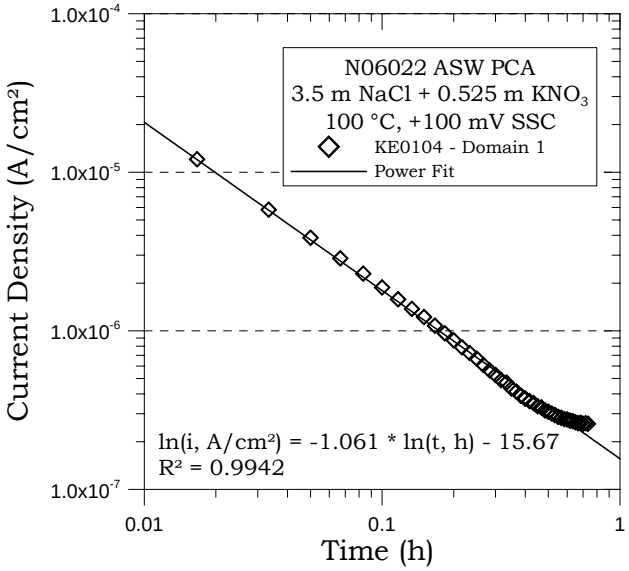

Figure 8. Power Law in Domain 1

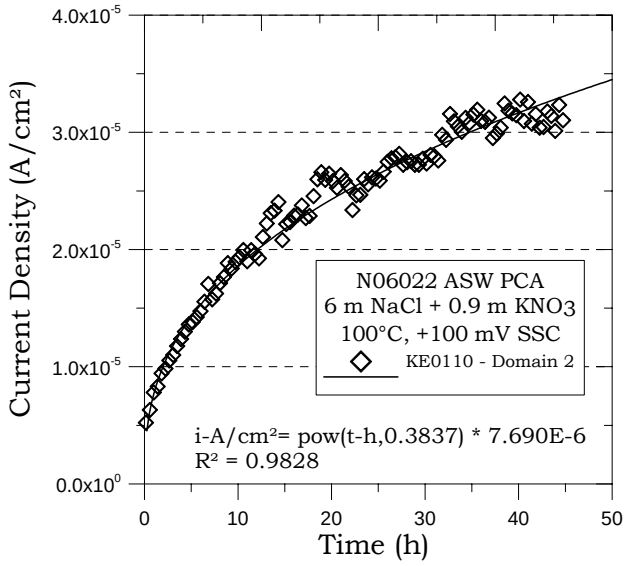

Figure 9. Power Law in Domain 2

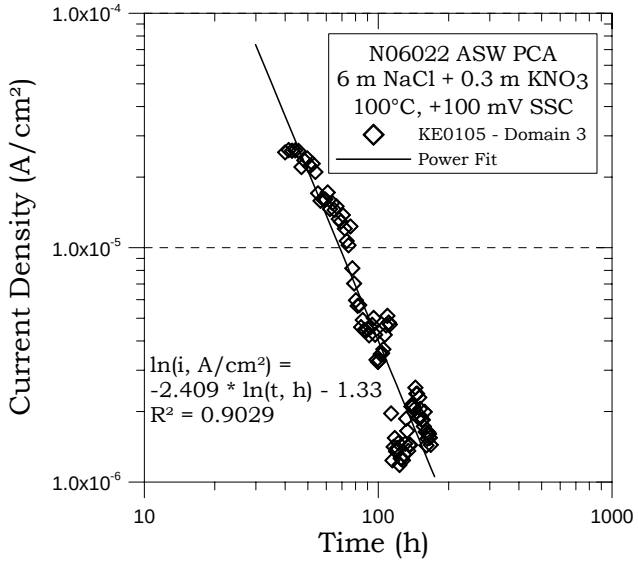

Figure 10. Power Law in Domain 3

Final Remarks

The current studies show that crevice corrosion can be initiated in an artificially creviced specimen of Alloy 22 when a constant potential between the breakdown potential and the repassivation potential is applied. The output current density shows three distinctive domains during the tests. In Domain 1 (which was the shortest), the current density decreased as the time increased. In Domain 1, the specimen showed an initial passivation at the anodic applied potential. In Domain 2, the current density increased as the time increased, initially faster and then slower, showing progressive stifling of crevice growth. In Domain 3, the activity in the corroded area decreased and the specimen regained its passivity. At the end of Domain 3, the current density was similar or lower than the current density at the initiation of Domain 1 where the specimen did not show crevice corrosion. In many instances the net current in Domain 3 was negative suggesting that the cathodic reduction of protons and/or nitrate inside the crevice was more important that the dissolution of the metal.

Crevice corrosion develops in Alloy 22 because a hydrochloric acid solution forms in the occluded areas of the specimen due to dissolution of the metal and subsequent hydrolysis. The corrosion rate of Alloy 22 in presence of hydrochloric acid is faster than in near neutral chloride plus nitrate brines outside the crevice former. The higher corrosion rate in hydrochloric acid is especially true in hot electrolytes (e.g., 100°C). It is likely that after the crevice corrosion attacked area reaches a certain critical size, the corrosion products would sequester the chloride ions thus the creviced electrolyte will become enriched in nitrate and its dissolution

will be governed by nitric acid rather than by hydrochloric acid. Therefore the corroding alloy inside the crevice will develop a passive film in the presence of nitric acid and a rapidly decreasing the dissolution rate. The presence of insoluble oxides (such as chromium, molybdenum and tungsten) will also act as a further barrier for crevice corrosion growth.

Current tests show that even though a constant driving force (applied potential) is imposed to the specimen, the extent of crevice corrosion growth is still limited. It is expected that natural redox potentials, which will control the corrosion potential as its solely driving force for crevice corrosion will be even less capable of promoting crevice growth.

CONCLUSIONS

- Crevice corrosion can be initiated in artificially creviced specimens of Alloy 22 if a constant potential is applied between the repassivation potential and the breakdown potential

- The output current density as a function of time has three characteristic domains, (1) passivation, (2) crevice corrosion nucleation and growth and (3) crevice corrosion stifling or repassivation.

- In all the tested conditions, crevice corrosion developed for a limited time before it died due to repassivation of the corroded area.

- The three domains of crevice corrosion can be explained using a power relationship between the output current and the testing time. The growth of crevice corrosion (Domain 2) has a positive exponent between 0.5 and 1.0.

- The repassivation of a growing crevice (Domain 3) is faster than the initial passivation before localized corrosion started (Domain 1).

- Electrolytes solutions with a higher nitrate to chloride ratio develop smaller crevice corrosion sites than electrolytes with a lower nitrate to chloride ratio.

ACKNOWLEDGMENTS

This work was partially performed under the auspices of the U. S. Department of Energy by the University of California Lawrence Livermore National Laboratory under contract W-7405-Eng-48. The work was supported by the Yucca Mountain Project, which is part of the DOE Office of Civilian Radioactive Waste Management (OCRWM).

DISCLAIMER

REFERENCES

1. R. B. Rebak, Paper 05610, Corrosion/2005 (NACE International, 2005: Houston, TX).
2. ASTM International, “Non Ferrous Alloys,” Standard B575, Volume 02.04 (ASTM, 2002: West Conshohocken, PA).
3. Haynes International, “Hastelloy C-22 Alloy”, Brochure H-2019E (Haynes International, 1997: Kokomo, IN).
4. R. B. Rebak in Corrosion and Environmental Degradation, Volume II, p. 69, Wiley-VCH, Weinheim, Germany (2000).
5. R. B. Rebak and P. Crook, Advanced Materials and Processes, February 2000.
6. Yucca Mountain Science and Engineering Report, U. S. Department of Energy, Office of Civilian Radioactive Waste Management, DOE/RW-0539, Las Vegas, NV, May 2001.
7. G. M. Gordon, Corrosion, 58, 811 (2002).
8. B. A. Kehler, G. O. Ilevbare and J. R. Scully, Corrosion, 1042 (2001).
9. K. J. Evans and R. B. Rebak in Corrosion Science – A Retrospective and Current Status in Honor of Robert P. Frankenthal, PV 2002-13, p. 344-354 (The Electrochemical Society, 2002: Pennington, NJ).
10. K. J. Evans, S. D. Day, G. O. Ilevbare, M. T. Whalen, K. J. King, G. A. Hust, L. L. Wong, J. C. Estill and R. B. Rebak, PVP-Vol. 467, Transportation, Storage and Disposal of Radioactive Materials – 2003, p. 55 (ASME, 2003: New York, NY).

11. S. D. Day, K. J. Evans and G. O. Ilevbare, in "Critical Factors in Localized Corrosion IV", PV 2002-24, p. 534 (The Electrochemical Society, 2003: Pennington, NJ).
12. D. S. Dunn, G. A. Cragnolino, and N. Sridhar, in Scientific Basis for Nuclear Waste Management XXIV, Vol. 608, p 89 (Materials Research Society, 2000: Warrendale, PA).
13. G. A. Cragnolino, D. S. Dunn and Y.-M. Pan, in Scientific Basis for Nuclear Waste Management XXV, Vol. 713, p 53 (Materials Research Society, 2002: Warrendale, PA).
14. V. Jain, D. Dunn, N. Sridhar and L. Yang, Corrosion/2003, Paper 03690 (NACE International, 2003: Houston, TX).
15. D. S. Dunn, L. Yang, Y. – M. Pan and G. A. Cragnolino, Corrosion/2003, Paper 03697 (NACE International, 2003: Houston, TX).
16. N. S. Meck, P. Crook, S. D. Day and R. B. Rebak, Corrosion/2003, Paper 03682 (NACE International, 2003: Houston, TX).
17. J. H. Lee, T. S. E. Summers and R. B. Rebak, Corrosion/2004, Paper 04692 (NACE International, 2004: Houston, TX).
18. D. S. Dunn, G. A. Cragnolino, Y. M. Pan and L. T. Yang, Corrosion/2004, Paper 04698 (NACE International, 2004: Houston, TX).
19. K. J. Evans, A. Yilmaz, S. D. Day, L. L. Wong, J. C. Estill and R. B. Rebak "Electrochemical Methods to Determine Crevice Corrosion Repassivation Potential of Alloy 22 in Chloride Solutions," JOM, January 2005 (TMS, 2005: Warrendale, PA).
20. K. J. Evans, L. L. Wong and R. B. Rebak "Determination of the Crevice Repassivation Potential of Alloy 22 by a Potentiodynamic-Galvanostatic-Potentiostatic Method," PVP-ASME Vol. 483, pp. 137-149 (American Society of Mechanical Engineers, 2004: New York, NY).
21. ASTM International, Volume 03.02, Standards G 5, G 15, G 48, G 59, G 61, G 102 (ASTM International, 2003: West Conshohocken, PA)
22. D. S. Dunn, Y.-M. Pan, K. Chiang, L. Yang, G. A. Cragnolino and X. He "Localized Corrosion Resistance and Mechanical Properties of Alloy 22 Waste Package Outer Containers" JOM, p. 49, January 2005 (TMS, 2005: Warrendale, PA)
23. G. O. Ilevbare, K. J. King, S. R. Gordon, H. A. Elayat, G. E. Gdowski and T. S. E. Summers "Effect of Nitrate on the Repassivation Potential of Alloy 22 in Chloride Containing Solutions," Presented at the Fall 2004 Meeting of the Electrochemical Society, 03-08Oct04, Honolulu, HI (to be published).

Table 1. Crevice Repassivation Potentials ER1 (in mV SSC) for ASW Artificially Creviced Alloy 22 MCA Specimens in deaerated NaCl + KNO_3 brines at 100°C [Ref. 23].

Electrolyte and Temperature	$[NO_3^-]/[Cl^-]$	$[Cl^-]/[NO_3^-]$	Repassivation Potentials (ER1) from CPP	Ave ER1 ± SD
1 m NaCl + 0.05 m KNO_3	0.05	20	-104, -116	-110 ± 6
1 m NaCl + 0.15 m KNO_3	0.15	6.67	21, -50	-15 ± 36
3.5 m NaCl + 0.175 m KNO_3	0.05	20	-119, -101	-110 ± 9
3.5 m NaCl + 0.525 m KNO_3	0.15	6.67	-68, -62	-65 ± 3
6 m NaCl + 0.3 m KNO_3	0.05	20	-85, -114	-100 ± 15
6 m NaCl + 0.9 m KNO_3	0.15	6.67	-75, -22	-49 ± 27
SSC = Saturated Silver Chloride electrode, ASW = As-Welded, MCA = Multiple Crevice Assembly, SD = Standard Deviation, ER1 = Potential at which the reverse current density in a CPP test is 1 μA/cm², CPP = Cyclic Potentiodynamic Polarization				

Table 2. Approximate Chemical Composition of the Materials Used for Testing

Element	Ni	Cr	Mo	W	Fe	Others
Nominal ASTM B 575	50-62	20-22.5	12.5-14.5	2.5-3.5	2-6	2.5Co-0.5Mn-0.35V max.
PCA Specimen Number and Heat						
KE0101-0150 Base Heat 059902LL2	59.56	20.38	13.82	2.64	2.85	0.16Mn-0.17V
KE0101-0150 Weld Wire Heat XX2048BG	59.4	20.48	14.21	3.02	2.53	0.2Mn
KE0151-0239 Base Heat 2277-0-3183	55.29	21.23	13.37	2.93	3.65	1.7Co-0.23Mn-0.14V
KE0151-0239 Weld Wire Heat XX1829BG	59.31	20.44	14.16	3.07	2.2	0.21Mn-0.15Cu

Table 3. Test Matrix and Results. Testing Temperature was 100°C.

Specimen	Electrolyte	$[NO_3^-]/[Cl^-]$	24 h E_{corr} (Deaerated Brines)	Ave CR ± SD (µm/year)	Applied Potential (mV SSC)	Constant Potential Results
KE0108	3.5 m NaCl + 0.175 m KNO_3	0.05	-454	0.4988 ± 0.0758	100	CC
KE0106		0.05	-550	1.4440 ± 0.1941	100	CC
KE0104	3.5 m NaCl + 0.525 m KNO_3	0.15	-559	0.5637 ± 0.0842	100	CC
KE0166		0.15	-414	5.6993 ± 0.3961	100	CC
KE0105	6 m NaCl + 0.3 m KNO_3	0.05	-514	0.2483 ± 0.0206	100	CC
KE0164		0.05	-311	0.9230 ± 0.1327	0	CC
KE0103	6 m NaCl + 0.9 m KNO_3	0.15	-535	1.3774 ± 0.3762	100	CC
KE0110		0.15	-59	6.7797 ± 0.1990	100	CC
E_{corr} = Corrosion Potential, CR = Corrosion Rate, SD = Standard Deviation CC = Crevice Corrosion						

Table 4. Results from Constant Potential Testing at 100°C.

Specimen	Time for Domain 1 (h)	Time for Domain 2 (h)	Time for Domain 3 (h)		Power Exponent Domain 1	Power Exponent Domain 2	Power Exponent Domain 3
KE0108	0.25	26.03	142		-0.742	0.536	-1.433
KE0106	0.17	14.17	154		-0.722	0.913	-1.467
KE0104	0.73	31.53	136		-1.061	1.042	-1.051
KE0166	NA	12.1	156		NA	0.568	-2.031
KE0105	0.81	40	127		-0.840	0.806	-2.409
KE0164	0.55	64	103		-0.612	0.505	-2.692
KE0103	0.75	23.3	144		-0.771	0.979	-0.492
KE0110	0.16	45	123		-0.079	0.384	-3.506

Table 5. Results from POT at 100°C.

Specimen	Total Charge (Coulomb)	Total Dissolved Mass (mg)	Total Depth (µm) (24 spots)	Total Depth (µm) (1 spot)
KE0108	319.04	76.98	59.06	1417.33
KE0106	260.28	62.80	48.18	1156.29
KE0104	124.75	30.1	23.09	554.20
KE0166	75.69	18.26	14.01	336.24
KE0105	94.61	22.83	17.51	420.29
KE0164	214.60	51.78	39.72	953.33
KE0103	88.04	21.24	16.30	391.10
KE0110	91.80	22.15	16.99	407.80